Earthquake-induced slope failure susceptibility in eastern Nepal

Ranjan Kumar Dahal

Geodisaster Research Center, Central Department of Geology
Kirtipur, Kathmandu, Nepal
Email: ranjan@tugeology.edu.np

ABSTRACT

Nepal is considered as one of the earthquake-prone countries in the region. Earthquake is a major concern of Nepal because of rapid population growth, poor land use planning, precarious settlement patterns, and poorly implemented building code. Earthquakes in Nepal have been reported since 1255 while major earthquakes were recorded in 1408, 1681, 1810, 1833, and 1866, 1934, 1980, 1988, 2011, and 2015. An earthquake in September 18, 2011 measuring 6.9 in Richter scale, killed 6 people and injured 30 people in Nepal. There were many roadside slope damages near the epicenter area. To assess the roadside slope damages after this earthquake, a field visit was conducted and a landslide inventory map along the roadside slope was prepared for most damaged area. This paper provides a comprehensive information about earthquake-induced slope failures occurred in the Mechi Highway of eastern Nepal and also discusses an approach of earthquake-induced slope failures hazard mapping in Nepal.

Keywords: Earthquake, slope failure, susceptibility, eastern Nepal

INTRODUCTION

Earthquake-induced slope failures are one of the most recurring phenomena during earthquake. Commonly, damage from earthquake-induced slope failures is worse than damage related to the shaking and rupture of the earthquake itself. In recent years, Geographic Information Systems (GIS) and remote sensing have significantly improved our ability to map earthquake-induced landslides. With the application of aerial photographs and field verifications, slope failures induced by earthquakes have been mapped and analyzed in California, El Salvador, Taiwan, Japan, Italy and Pakistan (e.g., Wilson and Keefer 1985, Harp and Keefer 1990, Harp and Jibson 1996, Jibson et al. 2000, Parise and Jibson 2000, Capolongo et al. 2002, Chigira et al. 2003, Chigira and Yagi 2006, Wang et al. 2007, Owen et al. 2008). Several methods have been developed for the evaluation of hazards represented by earthquake-induced landslides, including statistical analysis (Keefer 1984, 2000) and a deterministic method (Mankelow and Murphy 1998, Jibson et al. 2000, Luzi and Pergalain 2000, Carro et al. 2003), both of which aim to quantify earthquake-induced landslide susceptibility and hazard zonation. These studies have provided valuable information about the characteristics of earthquake-induced landslides.

When earthquake-induced slope failures in Nepal are concerned, there were many incidents and the record on the earthquake-induced slope failures is not well documented. Nepal lies in seismically active region and its history is full of devastating earthquakes. The major source of earthquakes in Nepal and the Himalayan Region is the subduction of the Indian plate underneath the Eurasian plate, resulting contraction effect, stress concentration. Seismicity is considered to be high in this region based on the frequency and strength of the past earthquakes. Seismicity of the Himalayan region has been studied in terms of its relationship with known geological faults and tectonic activities. During the past~19000 years, three great earthquakes were occurred along the Himalayan front. From east to west, the sequence includes the 1905 Kangra earthquake (Mw ~7.8), the 1934 Bihar-Nepal earthquake (Mw = 8.1), and the 1950 Assam earthquake (Mw ~8.6). After 1934 Bihar-Nepal earthquake in Nepal, eight major earthquake hit Nepal and last earthquake was Gorkha Earthquake (2015). Sikkim/Nepal border earthquake of September 18, 2011 hits eastern Nepal before Gorkha earthquake 2015. Although, USGS has named this earthquake as Sikkim/Nepal border earthquake, the earthquake epicenter lies in Nepalese territory and situated at north-east part of Taplejung district, near to the Kanchanjunga Base Camp (Fig. 1). In this earthquake, 14, 544 houses damaged (6, 435 completely destroyed), 6 people died and 30 people were injured in Nepal. The shake map produced by USGS immediate after earthquake (Fig. 1) suggests that the earthquake shaking was moderate to strong in east Nepal, Sikkim (India) and few part of south Tibet (China). During this earthquake, USGS and Department of Mines and Geology of Nepal measured the peak ground accelerations between 38 gal and 90 gal in the Koshi Highway region and 90 gal to 177 gal in the Mechi Highway region. As a result, there were many roadside slope damages along the Mechi Highway in comparison with the Koshi Highway. Many longitudinal as well as transverse cracks were also observed in the ridge part.

The main objective of this paper is to evaluate the earthquake-induced slope failure hazard mapping in Nepal. For this purpose, recently damaged area due to Sikkim/Nepal border of September 18, 2011 of eastern Nepal along the Mechi Highway is selected for the study and hazard zonation map is prepared.

STUDY AREA AND GEOLOGICAL SETTING

The Mechi highway is the major highway of far east Nepal and it connects mountains of north with the plain area (Terai) of south (Fig. 2). Especially, the northern part of Mechi Highway and the few part of Koshi Highway of east Nepal have been affected by earthquake-induced slope failures such as debris falls, debris slides and rock falls. Therefore, for this research a highly affected stretch of Mechi Highway (Fig. 2) is also selected for detail slope failure hazard mapping.

Geo-tectonically, Nepal is divided into five major tectonic zones, namely, Terai Zone, Siwalik Zone, Lesser Himalayan Zone, Higher Himalayan Zone and Tibetan-Tethys Himalayan Zone (Ganser 1964). These tectonic zones are separated by major thrusts and faults of the Himalaya and those faults and thrusts are named from north to south (Fig. 2) as South Tibetan Detachment System (STDS), Main Central Thrust (MCT), Main Boundary Thrust (MBT) and Main Frontal Thrust (MFT). Likewise, geomorphologically, Nepal is divided into eight units running east-west, namely, Terai, Churia Range, Dun Valley, Mahabharat Range, Midland, Fore Himalaya, Higher Himalaya, Inner and Trans Himalaya (Dahal and Hasegawa 2008).
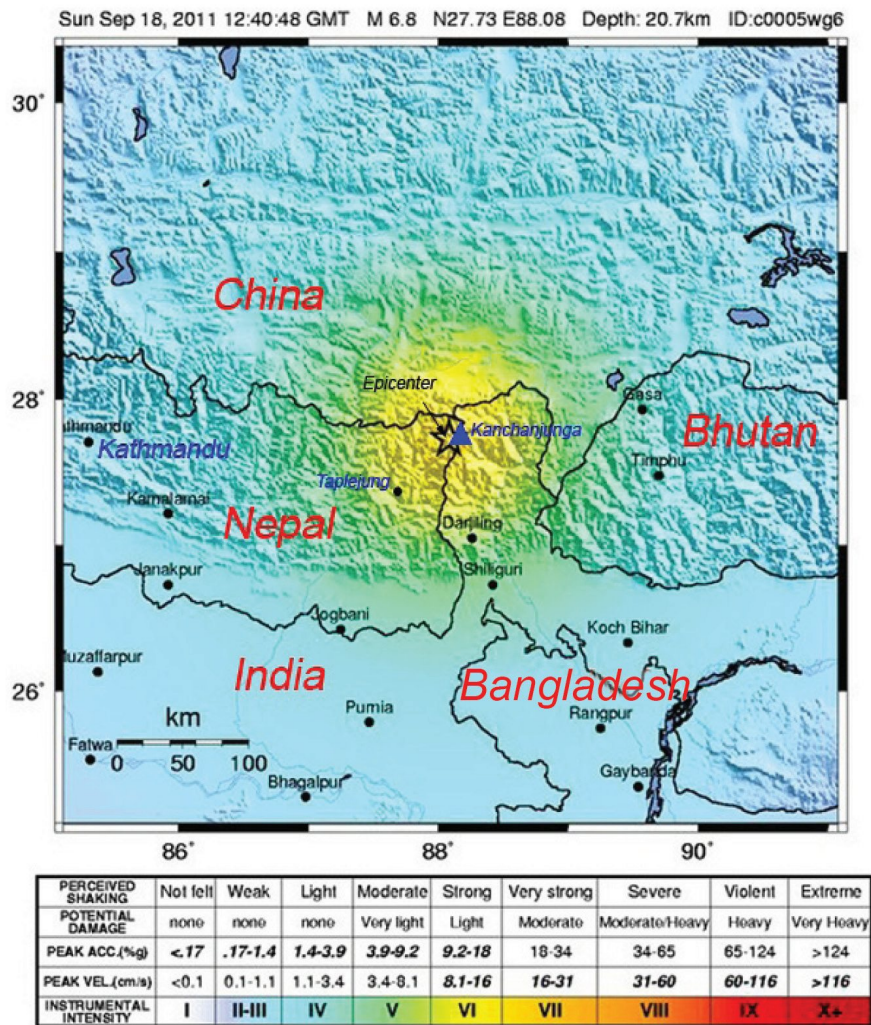
Fig. 1: Shake map of the Sikkim-Nepal Border Earthquake of September 18, 2011 (modified after USGS 2011).

East Nepal comprises of two tectonic units: a Lesser Himalayan Zone exposed in the window (young rocks, i.e. rocks of the Lesser Himalayan Zone is surrounded by old rocks, i.e. rocks of the Higher Himalayan Zone) and a thrust sheet propagated to the south, near to the MBT as Higher Himalayan Zone. The Lesser Himalayan Zone consists of mainly of phyllites, shcists, quartzite and augen gneiss of granitic origin with minor association of amphibolites, marbles exposed in the southern part. The Higher Himalayan Zone consists of mainly garnet, kyanite, sillimanite bearing banded high grade gneiss, inter-bedded with quartzite. As Mechi Highway has north-south extension, it runs through all geological zones of the Nepal Himalaya. Most part of the Mechi Highway passes through Higher Himalayan Zone, especially in the terrain of banded gneiss. Likewise, the northern parts of the highway situated in tectonic window and runs in quartzitic and phyllitic terrains belonging to the Lesser Himalayan Zone (Fig. 2). In many places of northern part, both highways are passing
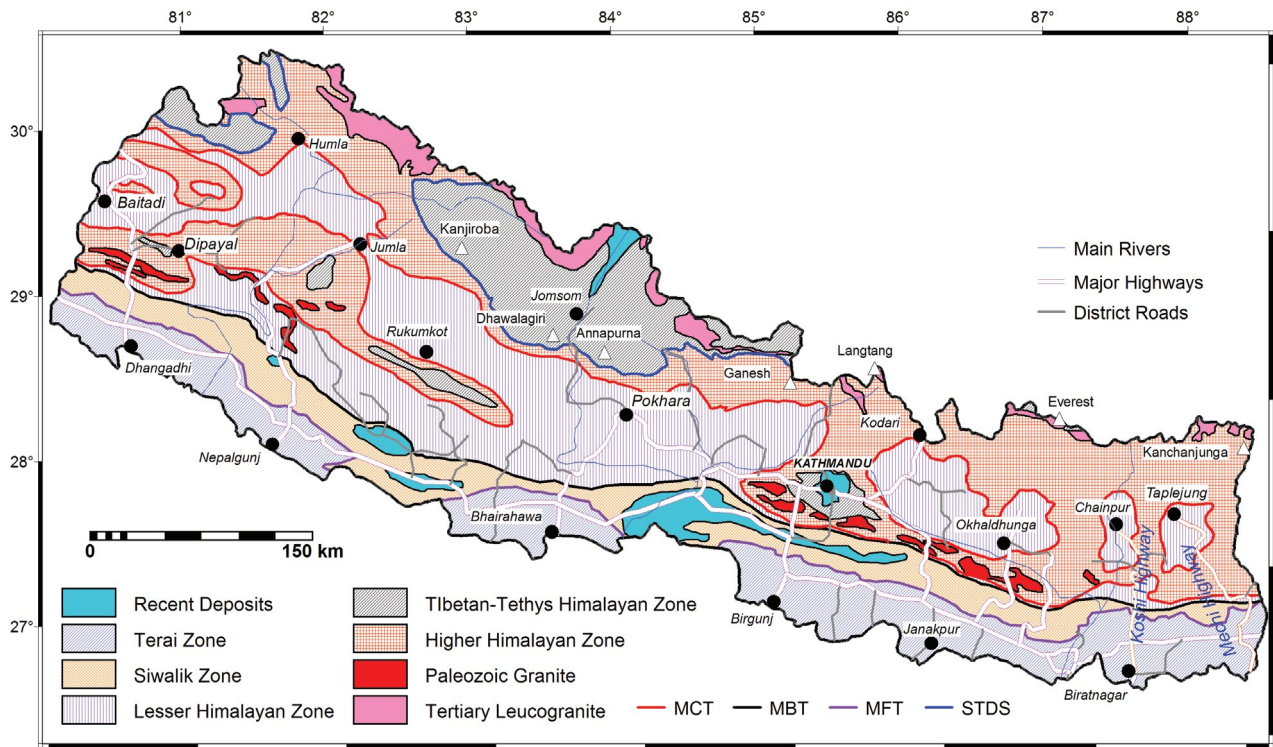
Fig. 2: Geological map of Nepal and location of Mechi and Koshi highways in east Nepal.

through steep slopes and ridges having elevation more than 2500 m.

Field visit was carried out in the study area in 2nd week of October (after 3 weeks of earthquake), 2011. Field visit immediately after earthquake was not possible because of damage in highways and relief support activities for earthquake victims. In total, four days were spent to inspect damages in the roadside slope of Mechi Highway (Fig. 3). Nearly 200 km stretch of Mechi Highway were visited from Charali to Taplejung. Out of whole section of highway, stretch between Ranke Bhanjyang-Phidim-Gopetar is found to be most affected section (Fig. 4). A slope failure inventory map was prepared in topographical base map. Most of the slope failures had failure depths of less than 2 m, and mostly translational to semi-rotational movement was evident on the failure plain. The slope failures are identified as earthquake induced slope failure as per the discussion of with local villagers. The area of the slope failures ranged from 93 sq. m to 10, 987 sq. m. In total 35 failures were identified. Slope failures inventory map and photographs of few representative slope failures are provided in Fig. 4. In this section of road, many transverse cracks were observed on ridges and houses were also damaged. According to villagers, the highway was blocked for 1 day after earthquake. During the field visit, the debris were observed on roadside free spaces and in the site of failure, only single lane was opened for traffic. Although there are no human casualties from the earthquake induced-slope failures in the area, the damages of roadside slope were intense in the section between Ranke Bhanjyang to Phidim.

TOPOGRAPHIC EFFECTS

The various investigations showed that topographic features are basically responsible for dissipation of seismic energy (e.g. Gilbert and Knopoff 1960) and extremely high accelerations are usually observed at sites located on topographic ridges (e.g. Davis and West 1973, Bannister et al. 1990, Geli et al. 1988, Ambraseys and Srbulov 1995, Miles and Keefer 2000, Lin et al. 2003, Uchida et al. 2004). Observations of the damage patterns of earthquakes, such as the 1987 Whittier Narrows, California earthquake, the 1989 Loma Prieta (California) earthquake, the 1994 Northridge, California earthquake, the 1999 Chi-Chi earthquake of Taiwan, the 2004 Chuetsu earthquake of Niigata Prefecture, Japan, and the 2005 Kashmir earthquake of Pakistan also indicate the occurrence of intense shaking in elevated ridges of rugged topography.

Geli et al. (1988) have reported that buildings on crests suffer more damage than those located at the base and they conclude that there is always significant amplification of frequencies corresponding to wavelengths about equal to mountain width at hilltops with respect to the base. In the case of September 18 Earthquake, It is quite well observed in Ranke Bhanjyang village, along the Mechi Highway. Many houses on the ridges were damaged and many cracks were observed on ridge (Fig. 4). Similarly, an amplification-deamplification pattern on slopes leads to a strong energy differential on the upper part of the slope. For the case of the Chi-Chi earthquake, Lin et al. (2003) mentioned that landslide frequency is much higher on or near the crests of hills. To evaluate topographic
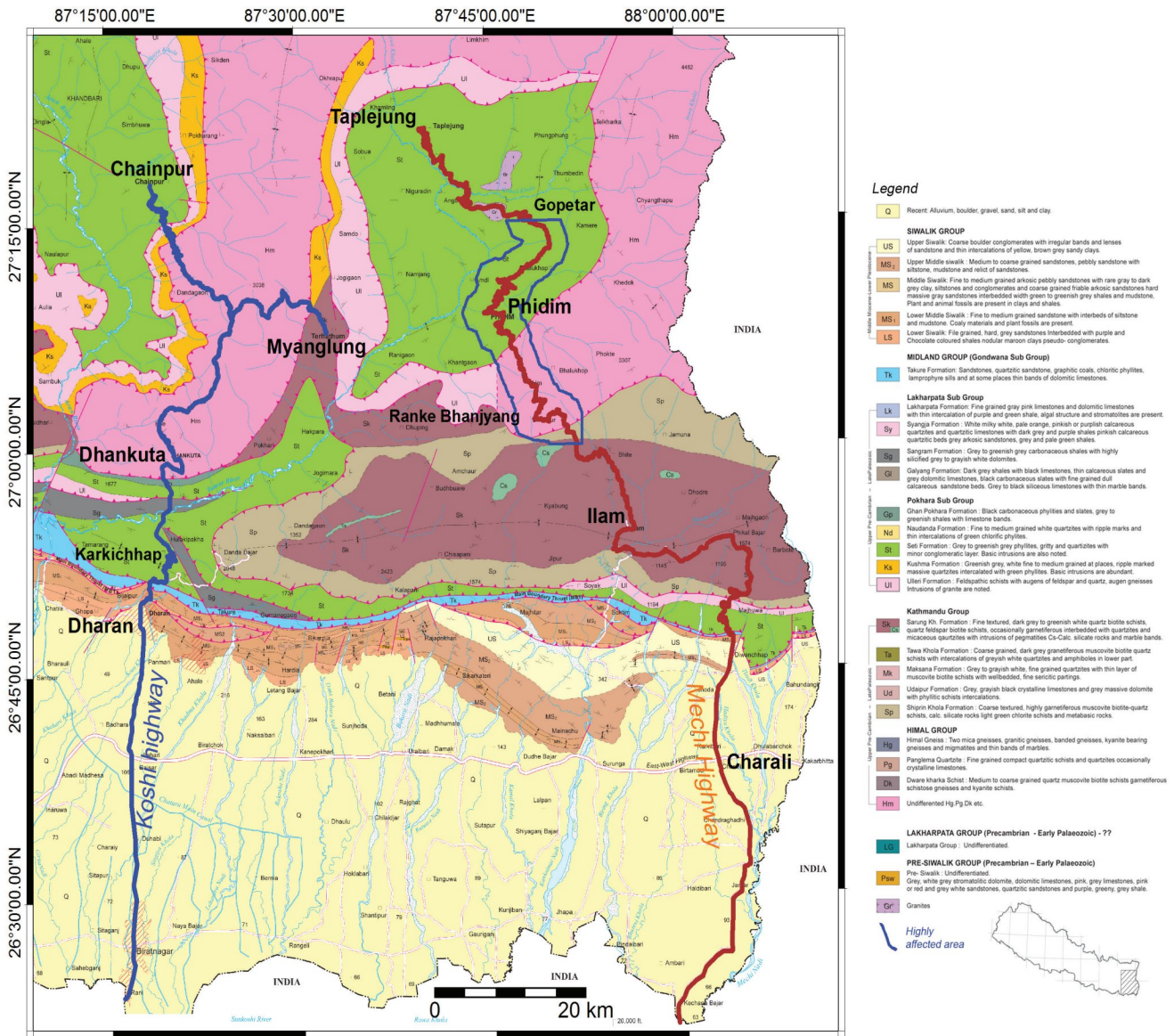
Fig. 3: Detail geological map of the study area (modified after DMG 2011).

effect in the study area, the topographic curvature of stretch between Ranke Bhanjyang to Gopetar (see Fig. 4) is calculated in GIS and cross checked with the landslide inventory. Digital contour data obtained by Department of Survey, Government of Nepal, is used to prepare Digital Elevation Model (DEM) of 20 m pixel size in this research. In total, 75% of earthquake-induced slope failures are found on ridge slope pixel and 25% were found on valley slope pixel. This simple evaluation clearly supports that in the Himalayan slopes also, frequency of earthquake-induced slope failure is much higher on or near the crests of hills.

HAZARD ZONING

The method proposed by Uchida et al. (2004, 2006) was used in this study to perform an earthquake-induced slope failure susceptibility analysis within the GIS platform. Taro Uchida and his team extensively studied landslide damage in the Rokko mountain region (granitic terrain) after the

Hanshin-Awaji Earthquake (Kobe earthquake) of 1995. They derived a landslide probability function based on discriminant analysis using slope, average curvature and maximum ground acceleration (Uchida et al. 2004, 2006) without considering geology and other intrinsic factors. Uchida et al. (2004) defined average curvature as the average of the maximum and minimum curvatures of all geodesics on the curved slope. In raster GIS, the average curvature, ε, can be derived from the following relationship:

$$\varepsilon = \frac{\dfrac{\partial^2 f}{\partial x^2}\left\{1+\left(\dfrac{\partial f}{\partial y}\right)^2\right\}+\dfrac{\partial^2 f}{\partial y^2}\left\{1+\left(\dfrac{\partial f}{\partial x}\right)^2\right\}-2\dfrac{\partial f}{\partial x}\dfrac{\partial f}{\partial y}\dfrac{\partial^2 f}{\partial x\partial y}}{\sqrt{2\left(1+\left(\dfrac{\partial f}{\partial x}\right)^2+\left(\dfrac{\partial f}{\partial y}\right)^2\right)^3}}$$

(1)

where f is the pixel value of a DEM generated from the contour map and x and y are the local coordinates. Concave slope gives a positive curvature value and convex slope gives
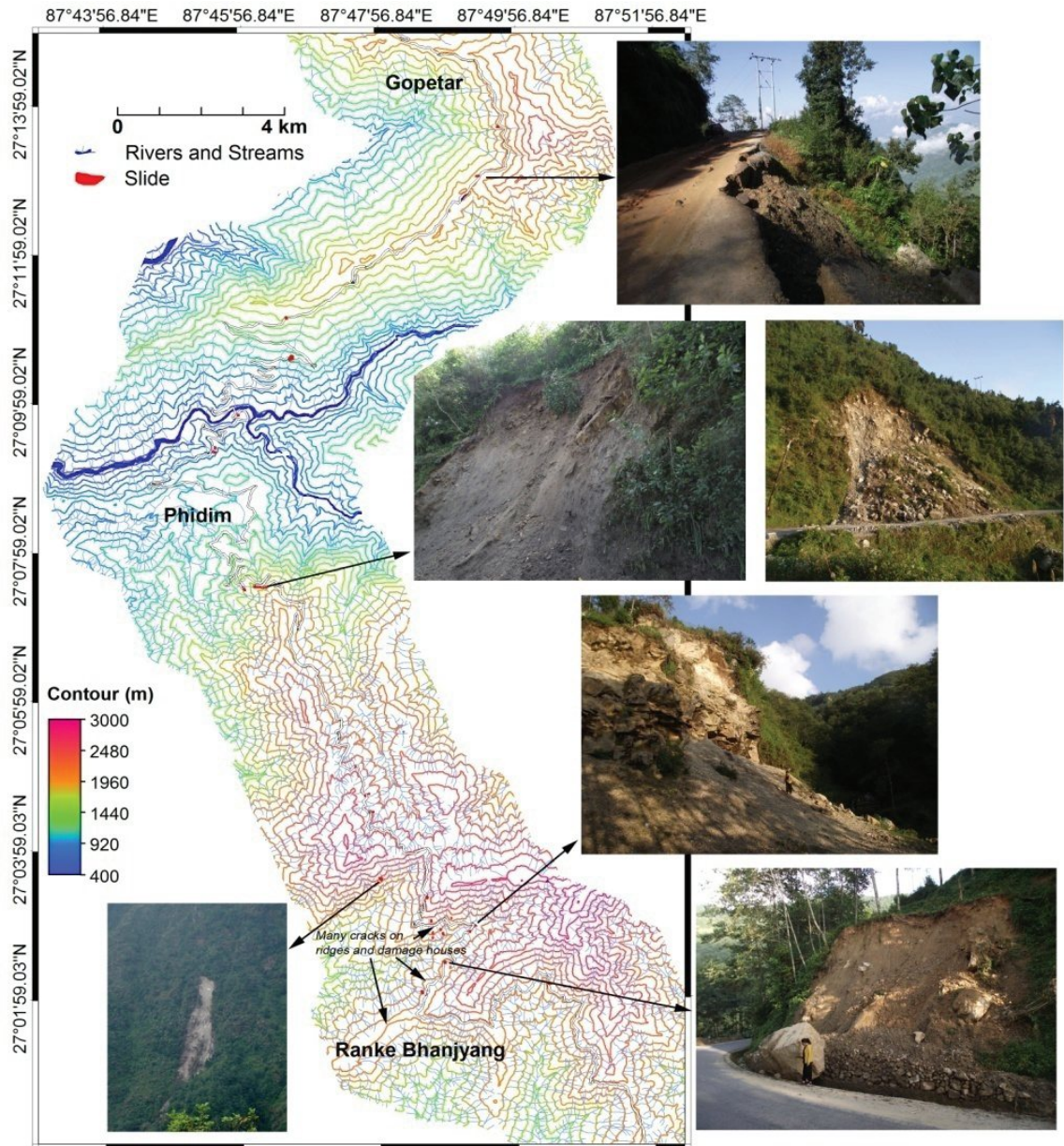
Fig. 4: Highly damaged road sections of the Mechi Highway and representative slope failures on roadside slope.

a negative curvature value. On the basis of average curvature defined in Eq. (1), Uchida et al. (2004) derived the landslide probability function from discriminant analysis as follows:

$$F = 0.075[\theta] - 8.9[\varepsilon] + 0.0056[a_{max}] - 3.2 \qquad (2)$$

where F is the landslide probability function or discriminant score, θ is the slope angle in degrees, ε is the average curvature, and slope failure is the maximum ground acceleration in gal (1 gal = 0.01 m/s^2). Pixels having positive F-value always have the potential to fail during an earthquake, and negative F-values suggest the slope will not fail during an earthquake. Equations (1) and (2) are easily applicable to DEM in the GIS platform.

The calculated F-value for the selected area does not have any correlation with the earthquake-induced slope failure in the area. To overcome this issue and to check the predictive power of F for slope failure occurrence, the F-values were qualitatively examined with the help of success rate curves. In statistical landslide susceptibility analysis, the success rate is a measure of goodness of fit and for this research, success rate can be a measure of the predictive power of landslide susceptibility values (here, F-values) because calculated susceptibility values do not have any statistical relationship with existing slope failures (as they do in other statistical landslide susceptibility analysis techniques). To obtain the success rate curve for the F-values, the calculated index values of all pixels in the map were sorted in descending order. The ordered pixel values were subsequently categorised into 100

classes with 1% cumulative intervals and an *F*-value map was prepared. The *F*-value map was crossed with the slope failure inventory map and the success rate curve was prepared from cross table values.

For the earthquake-induced slope failure after September 18, 2011, Sikkim/Nepal border earthquake, the success rate reveals that in 20% of the study area, *F*-values had a high rank and could explain 64% of total landslides. Likewise, 40% of higher slope failure hazard index (LHI) values could explain 95% of all existing landslides. Fig. 5 provides percent coverage of slope failures as a function of *F*-value. To compare the slope failure susceptibility values, the area under the curves are estimated from the success rate graphs (Fig. 5). The area under the curve qualitatively measures the success rate or prediction rate of the *F*-values. A total area equal to one denotes perfect prediction accuracy. Alternatively, when the area under the curve is less than 0.5000, the analysis is invalid. In this study, the area under the curve is 0.8344, indicating that the prediction rate was 83.44% (Fig. 5) and the analysis is valid.

To construct the classified susceptibility map of the selected small area, the reference success rate curve (Fig. 6) is created, and the corresponding *F*-values for susceptibility levels of 40%, 60%, 80% and 90% (with F-values ranging from low to high) are calculated. Four slope susceptibility classes are established as Stable Zone (less than 40%), Moderately Stable Zone (40-60%), Quasi Stable Zone (60-80%), and Unstable Zone (80-100%). The susceptibility map of the selected area prepared based on these intervals is shown in Fig. 6.

When the zonation map is crossed with slope failure map inventory map of the same area, it is noticed that in 96% of earthquake-induced slope failures after Sikkim-Nepal Border Earthquake of September 18, 2011 are found in Unstable and Quasi Stable zones (Fig. 7).
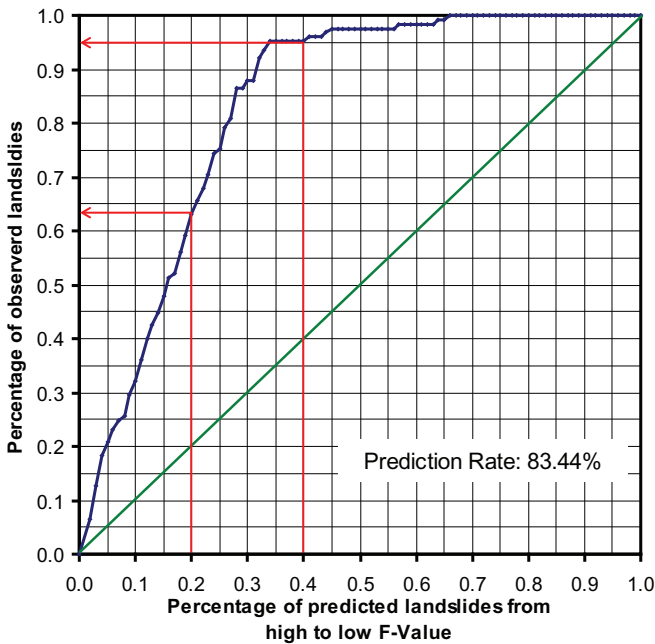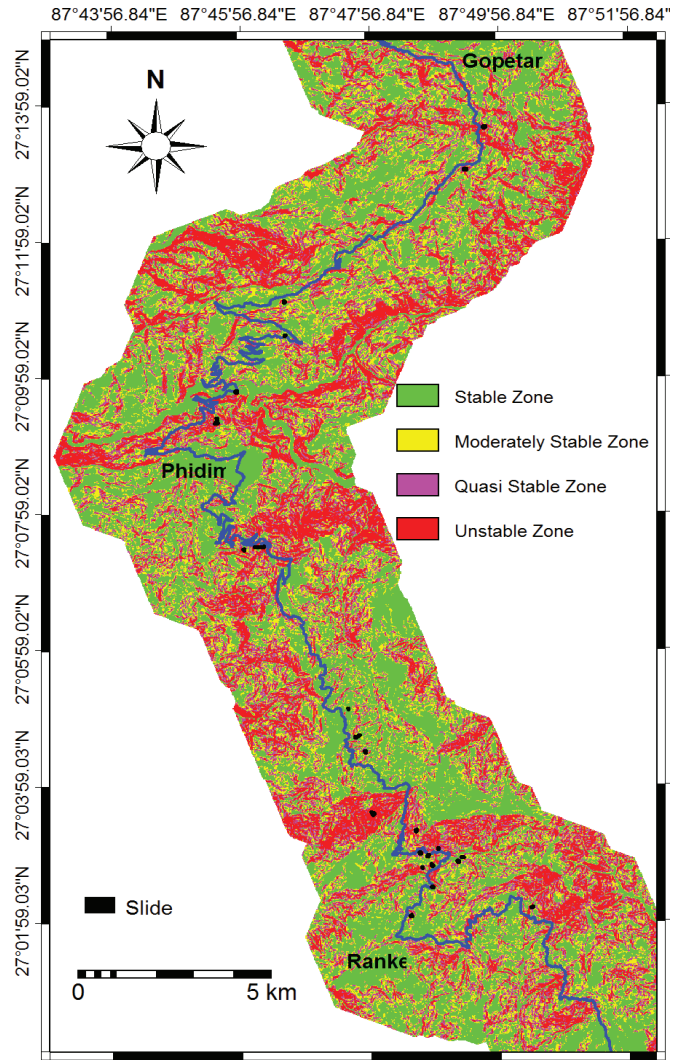

Fig. 6: Susceptibility map of the small selected area of Ranke-Phidim area. Slope failure after the September 18 2011 Sikkim/Nepal border earthquake are also shown on the map.

Fig. 5: Success rate curve and prediction rate of susceptibility map for the selected small area.
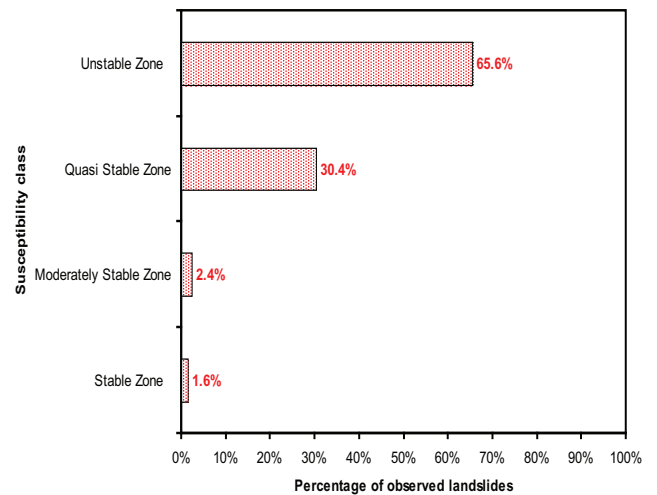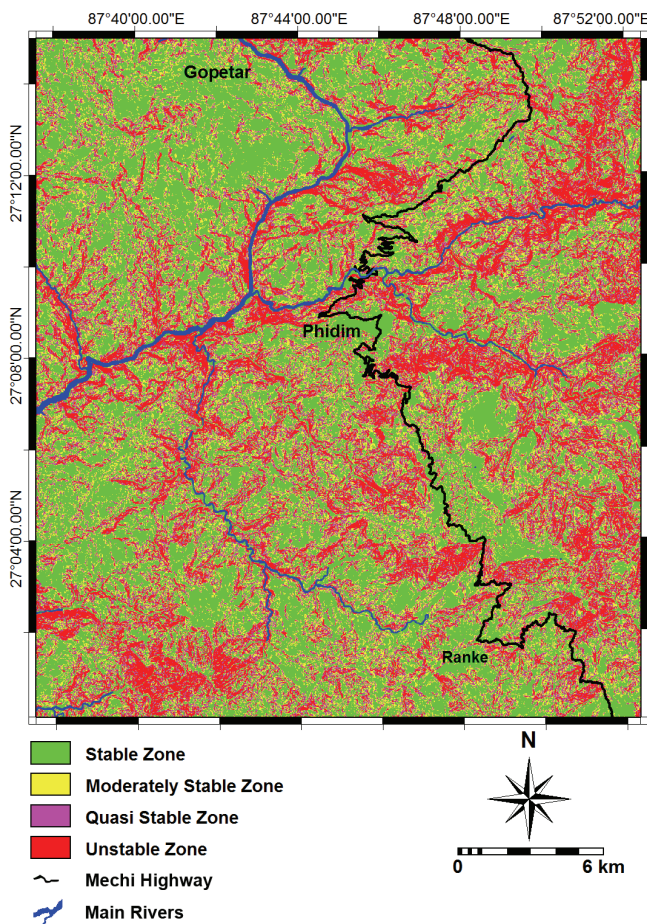

Fig. 7: Distribution of existing slope failures in small selected area. In total, 96% of earthquake-induced slope failures after Sikkim-Nepal Border Earthquake of September 18, 2011 are found in Unstable and Quasi Stable zones.

FINAL HAZARD MAP

The predictive power (83.4% accuracy, see Fig. 5) of the F-value calculated for the study area clearly suggests that the method proposed by Uchida et al. (2004) is reasonably accurate for the Nepal Himalaya also, although few intrinsic parameters are used in the analysis and the method is absolutely dependent on DEM. The success rate of slope failure susceptibility and hazard analyses of both rainfall-induced and earthquake-induced slope failures generally ranges from 75% to 85%. In such statistical analyses many intrinsic parameters are necessary (for example, geology, slope aspect, soil depth, soil type, land use, distance to road, distance to shore, distance to drainage, etc.), and data procurement can be extremely challenging. However, the method proposed by Uchida et al. (2004) requires only slope and curvature available from precisely-generated DEM data, and there is no need to consider any other intrinsic parameters. The maximum ground acceleration from earthquake shaking, which is site-specific, can be input as an approximation. Given the available data from previous earthquakes in a particular area, the recorded or probable future maximum ground acceleration can be used for hazard analysis in the area. In this work, a susceptibility map with more than 83% accuracy was obtained using only three parameters. This result is very encouraging, suggesting that the method proposed by Uchida et al. (2004) is useful for evaluating the probability of earthquake-induced slope failure in any area. The resultant earthquake-induced slope failure hazard map of the entire study area, given in Fig. 8, can be utilized for earthquake-induced slope failure susceptibility evaluation, planning, and preparation in the study area. The geology and geomorphological setting of the small selected area and the entire region are similar, and the final hazard map can be considered the most accurate earthquake-induced landslide hazard map of the study area.

CONCLUSIONS

This study evaluates features of the earthquake-induced slope failures in the Nepal Himalaya, which were occurred after September 18, 2011 Sikkim/Nepal Boarder Earthquake. Primarily, the study concludes that the Nepal Himalaya has great risk of earthquake-induced slope failures and the mountainous roads passing through the highly elevated Himalayan ridges are always subjected to damages in the events of great earthquakes. For the earthquake-induced slope failure hazard zonation, a methodology proposed by Uchida et al. (2004) in Japan is applied in the mountainous terrain of eastern Nepal also. The zonation map shows more than 80% accuracy and it is found that the methodology proposed by Uchida et al. (2004) is quite useful for the Nepal Himalaya also.

Fig. 8: Final-DEM based earthquake-induced slope failure susceptibility map of the Ranke-Phidim-Gopetar area. Given the prediction rate of the susceptibility map of small selected area (see Fig. 5 and Fig. 6), the accuracy of this final susceptibility map is also more than 80%.

REFERENCES

Ambraseys, N. and Srbulov, M., 1995, Earthquake induced displacement of slopes. Soil Dyn. Earthqu. Eng., v. 14, pp. 59–71.

Bannister, S. C., Husebye, E. S. and Ruud, B.O., 1990 Teleseismic P coda analyzed by three-component and array techniques: deterministic location of topographic P-to-Rg scattering near the NORESS array. Bull. seism. Soc. Am., v. 80, pp. 1969–1986.

BCDP, 1994, Building Code Development Project: Seismic Hazard Mapping and Risk Assessment for Nepal. UNDP/UNCHS (Habitat) Subproject: NEP/88/054/21.03. Min. Housing Phy. Planning, Kathmandu.

Capolongo, D., Refice, A. and Mankelow, J., 2002, Evaluating earthquake-triggered landslide hazard at the basin scale through GIS in the upper Sele river valley. Surveys in Geophysics, v. 23, pp. 595–625.

Carro, M., De Amicis, M., Luzi, L. and Marzorati, S., 2003, The application of predictive modeling techniques to landslides induced by earthquakes: the case study of the 26 September 1997 Umbria-Marche earthquake (Italy). Eng. Geol., v. 69(1-2), pp.139–159.

Chávez-García, F. J., Sanchez, L. R. and Hatzfeld, D., 1996, Topographic Site Effects and HVSR, A Comparison between Observation and Theory. Bull. Seism. Soc. Am.,

v. 86(5), pp. 1559–1573.

Chigira, M. and Yagi, H., 2006, Geological and geomorphological characteristics of landslides triggered by the 2004 Mid Niigta prefecture earthquake in Japan. Eng. Geol, v. 82, pp. 202–221.

Chigira, M., Wang, W. N., Furuya, T., Kamai, T., 2003, Geological causes and geomorphological precursors of theTsaoling landslide triggered by the 1999 Chi-Chi Earthquake, Taiwan. Eng. Geol., v. 68. Pp. 259–273.

Dahal, R. K. and Hasegawa, S., 2008, Representative rainfall thresholds for landslides in the Nepal Himalaya. Geomorphology, v. 100(3-4), pp. 429–443.

Davis, L. L. and West, L. R., 1973, Observed effects of topography on ground motion. Bull. Selsm. Soc. Amer., v. 63, pp. 283–298.

DMG, 2011, Geological Map of Eastern Nepal. Department of Mines and Geology, Lainchaur, Kathmandu, Nepal.

Gansser, A. 1964, Geology of the Himalayas. London Wiley Interscience, 289 p.

Geli, L., Bard, P. Y. and Jullien, B., 1988, The effect of topography on earthquake ground motion: a review and new results. Bull. Seism. Soc. Am., v. 78(1), pp. 42–63.

Gilbert, F. and Knopoff, L., 1960, Seismic Scattering from Topographic irregularities. Jour. Geophys. Research, v. 65, pp. 3437–3444.

Harp, E. L. and Jibson, R. W., 1996, Landslides triggered by the 1994 Northridge, California earthquake. Seismol. Soc. Am. Bull., v. 86(1B), pp. S319–S332.

Harp, E. L. and Keefer, D. K., 1990, Landslides triggered by the earthquake. *In*: Rymer, M. J. and Ellsworth, W. L. (eds.), The Coalinga, California, earthquake of May 2, 1983, U.S. Geol. Surv. Professional Paper, v. 1487, pp. 335–347.

Hasegawa, S., Dahal, R. K., Yamanaka, M., Bhandary, N. P., Yatabe, R. and Inagaki, H., 2009, Causes of large-scale landslides in the Lesser Himalaya of central Nepal. Envir. Geol., v. 57(6), pp.1423–1434.

Jibson, R. W., Harp, E. L. and Michael, J. A., 2000, A method for producing digital probabilistic seismic landslide hazard maps. Eng. Geol., v. 58, pp. 271–290.

Keefer, D. K., 1984, Landslides caused by earthquakes. Geol. Soc. Am. Bull., v. 95, pp. 406–421.

Keefer, D. K., 2000, Statistical analysis of an earthquake-induced landslide distribution – the 1989 Loma Prieta.

California event, Eng. Geol., v. 58(3-4), pp. 231–249.

Lin, C.-W., Shieh, C.-L., Yuan, B.-D., Shieh, Y.-C., Liu, S.-H. and Lee, S.-Y., 2003, Impact of Chi-Chi earthquake on the occurrence of landslides and debris flows: example from the Chenyulan River watershed, Nantou, Taiwan. Eng. Geol., v. 71, pp. 49–61.

Luzi, L. and Pergalani, F., 2000, A correlation between slope failures and accelerometric parameters: the 26 September 1997 earthquake (Umbria– Marche, Italy). Soil Dyn. Earthqu. Eng., v. 20, pp. 301–313.

Mankelow, J. M. and Murpy, W., 1998, Using GIS in the probabilistic assessment of earthquake triggered landslide hazards. Jour. of Earthquake Eng., v. 2(4), pp. 593–623.

Miles, S.B. and Keefer, D. K., 2000, Evaluation of seismic slope-performance models using a regional case study. Envir. and Eng. Geosci., v. 6(1), pp. 25–39.

Owen, L. A., Kamp, U., Khattak, G. A., Harp, E. L., Keeferd, D. K. an Bauer, M. A., 2008, Landslides triggered by the 8 October 2005 Kashmir earthquake. Geomorphology, v. 94, pp.1–9.

Parise, M. and Jibson, R. W., 2000, A seismic landslide susceptibility rating of geologic units based on analysis of characteristics of landslides triggered by the 17 January, 1994 Northridge, California earthquake. Eng. Geol., v. 58, pp. 251–270.

Uchida, T., Kataoka, S., Iwao, T., Matsuo, O., Terada, H., Nakano, Y., Sugiura, N. and Osanai, N., 2004, A study on methodology for assessing the potential of slope failures during earthquakes. Technical note of National Institute for Land and Infrastructure Management, 91 p. (in Japanese with English summary).

USGS, 2011, Summary of Sikkim/Nepal Boarder Earthquake, 2011, September 18 available in http://earthquake.usgs. gov/earthquakes/pager/events/us/c0005wg6/index. html#summary

Wang, H. B., Sassa, K. and Xu, W. Y. 2007, Analysis of a spatial distribution of landslides triggered by the 2004 Chuetsu earthquakes of Niigata Prefecture, Japan. Nat. Haz., v. 41, pp. 43–60.

Wilson, R. C. and Keefer D. K., 1985, Predicting areal limits of earthquake-induced landsliding. In: Ziony, J. I. (Ed.), Evaluating Earthquake Hazards in the Los Angeles Region - An Earth-science Perspective. US Geol. Surv. Prof. Paper, v. 1360, pp. 316–345.